13th IEA Heat Pump Conference
April 26-29, 2021 Jeju, Korea

Development and Lab-scale Performance Evaluation of a High Temperature Heat Pump for Integration into a Power-to-Heat to-Power System

Miguel Ramirez[a*], Felipe Trebilcock[a], Xabier Peña[a], Asier Martinez-Urrutia[a], Abdelrahman H. Hassan[b,c]

[a]Tecnalia Research & Innovation, Energy and Environment Division, Area Anardi 5, Azpeitia, Guipuzkoa 20730, Spain.
[b]Instituto Universitario de Investigación en Ingeniería Energética, Universitat Politècnica de València, 46022, Valencia, Spain.
[c]Mechanical Power Engineering Department, Faculty of Engineering, Zagazig University, Zagazig 44519, Egypt.

Abstract

Power-to-heat-to-power systems are an interesting approach to deal with the intermittent power generation from renewable energy sources. However, storing heat requires large storage volume and associated heat losses decrease the system performance. High Temperature Heat Pump (HTHP) systems can operate during surplus power generation periods storing heat in a latent heat storage and discharge it to drive a heat engine for electricity generation. The presented work has been performed under the frame of the EU funded CHESTER project (www.chester-project.eu) in which the performance of this technology is assessed. This paper presents the experimental study of a HTHP which will be integrated into a Compressed Heat Energy STorage (CHEST) system. A Low Global Warming Potential (GWP) working fluid is implemented and the configuration cycle is selected to optimize the charging conditions of a latent heat storage. The operating temperatures of the HTHP are set from 72°C to 105°C in the heat source side. The heat sink temperature is set at 133°C that corresponds to the melting point of the phase change material.

Selection and/or peer-review under responsibility of the organizers of the 13th IEA Heat Pump Conference 2020.

Keywords: High Temperature Heat Pump; Compressed Heat Energy Storage; Reciprocating Compressor; Low Global Warming Potential fluids; R1233zd(E);

1. Introduction

The amount of electricity produced by renewable energy systems in the EU reached 30% of the total gross electricity consumption in 2016. Hydro and wind power play a key role in the renewable power market contributing with 36.9% and 31.8% respectively of the total renewable power consumed [1]. However, the intermittent nature of renewable energy sources poses a challenge to overcome the successful coverage of the electricity network. Electricity storage systems are expensive and the existing technologies cannot satisfy the demand requirements of the grid at an affordable cost [2].

Other concepts of large-scale power storage systems are pumped hydro storage (PHS), compressed air energy storage (CAES), and pumped thermal electricity storage (PTES). PHS dominates the electricity storage market with 96% of the total stored capacity worldwide. It requires large water reservoirs and high height of elevation between the reservoirs. CAES is also depending on geographical characteristics of the area since it requires underground reservoirs [3]. PTES systems have been implemented in solar power systems being the second larger electricity storage technology [4]. Thermal storage presents lower cost than electricity storage systems and with an attractive life expectancy that can reach 10,000 cycles of operation [5].

* Corresponding author. Tel.:+34-946-430-850; fax: +34-946-430-850.
E-mail address: Miguel.ramirez@tecnalia.com

PTES systems can present different configurations and various combination of systems have been proposed in the literature. A combination of heat pump, thermal storage and organic Rankine cycle (ORC) can results in high roundtrip efficiency when the heat source temperature of the heat pump is higher than the condensing temperature of the ORC. Roundtrip efficiencies can reach values equivalent to 1.3 for heat source temperatures from 80° to 110°C and using R-1233zd(E) as working fluid [6]. Another similar concept the called Compressed Heat Energy STorage (CHEST) system has presented power ratio values of 1.25 operating with 100°C heat source temperature and 15°C of heat sink in the ORC side [7].

Nomenclature

COP	Coefficient of performance, [-]
cp	Specific heat capacity, [kJ/kg°C]
f	Frequency, (Hz)
h	Enthalpy, [kJ/kg]
m	Mass flow rate, [kg/s]
n	Number of pistons
P	Power, [kW]
Q	Heat capacity, [kW]
T	Temperature, [°C]
W_{in}	Electric power consumption, [kW]

Greek letters

Δ	Difference, [-]
η	Efficiency, [%]

Subscripts

dis	Discharge
displ	Displacement
el	Electric
in	Inlet
is	Isentropic
out	Output
r	Refrigerant
su	Suction
vol	Volumetric
w	Water

Abbreviations

CAES	Compressed air energy storage
CHEST	Compressed Heat Energy Storage
GWP	Global Warming Potential
HCFO	Hydrochlorofluoro-olefin
HFO	Hydrofluoro-olefin
HTHP	High Temperature Heat Pump
LH-TES	Latent Heat Thermal Storage
SH-TES	Sensible Heat Thermal Storage
ORC	Organic Rankine Cycle
PHS	Pumped hydro storage
PTES	Pumped thermal electricity storage

2. The CHESTER project

The CHEST system of this study is a combination of Rankine cycles and a latent heat storage unit that can use either water or organic media as working fluid [5]. The system is activated via high temperature heat generated from low temperature heat via a thermal cycle (heat pump). The high temperature heat generated charges the latent heat thermal energy storage (LH-TES). Sensible heat could be also stored in a sensible heat thermal energy storage (SH-TES) to optimize the cycle. Then during power demand periods heat from both the LH-TES and SH-TES storages is discharged to drive a heat engine cycle, in this case is an organic Rankine cycle (ORC), to generate electricity. This is an attractive concept to operate when cheap electricity and low temperature heat is available to cover power demand during high demand periods.

The aim of the CHESTER project is to develop and validate via a small-scale CHEST system of 10kWe the possibility to store power in heat and to deliver it as power minimizing losses. This system is destinated to store excess power from the generation of RES into thermal storage systems and to deliver it as electricity when demanded. The four main sub-systems developed for the CHEST system are the HTHP, the LH-TES along with the SH-TES, the ORC, and an isobaric expansion engine that will minimize the power consumption of the ORC system. The schematic diagram presented in Fig. 1 shows the basic configuration of the system and heat and power flows.

The heat source temperature of the CHEST prototype ranges from 60 to 100°C and the LH-TES charging temperature is in the range of 133-145°C. Therefore, these temperatures are considered as the heat source and heat sink of the HTHP, respectively. For these high temperature operating conditions, specialized components must be implemented such as compressor, refrigerant, lubricant, expansion device and others.

On the ORC side the heat source temperature is designed to be 133-145°C. In the in the dissipation side the temperature of the sink is in the range between 10 to 40°C. The operation of the ORC cycle is not analyzed in this study.

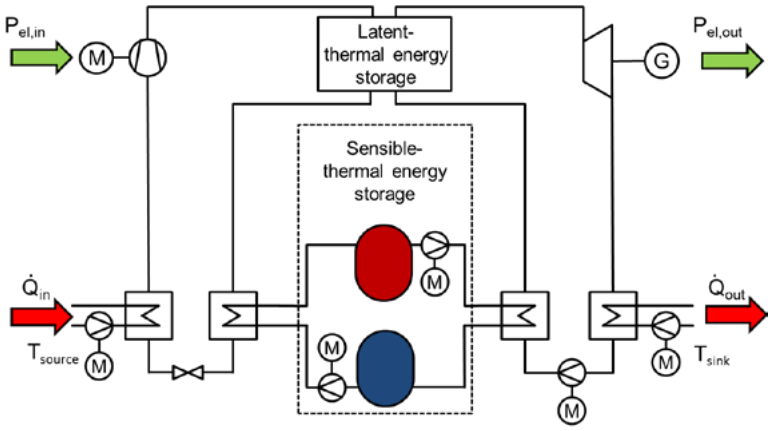

Fig. 1. Schematic diagram representing the CHEST system concept [8].

3. Testing method

For this study a water-to-water heat pump has been considered. Water flow temperatures can be controlled to simulate the operating conditions of the Chester project prototype. The water temperature is controlled in the source and both sink sides, the latent and the sensible.

The testing conditions and periods are selected according to the objectives of this study and the very high operating temperatures. Heat source water temperatures from 70° to 105°C are selected to obtain the performance curves at different temperature conditions of the source. In the sink side the water outlet temperature is maintained steady at approximately the melting point of the phase change material (133°C) and with the minimum experimentally possible temperature difference between inlet and outlet. In this way it is possible to simulate the operation of the HTHP during the charging of the LH-TES. In the subcooler the ΔT between the fluid inlet and outlet is maintained between 50 to 70 K by controlling the water inlet temperature. All water flow rates in the secondary circuits were maintained stable during each test.

During charging of the LH-TES the heat transfer coefficient will drop decreasing the capacity needed at the condensing. To match the heat pump´s heating capacity with the charging capacity of the LH-TES partial load can be applied. This is achieved via a speed drive (inverter) which controls the compressor speed and can drop the heating capacity of the heat pump. To measure the compressor capacity at part load conditions three compressor speeds were chosen for the testing campaign between 1000 to 1500 rpm.

It is also considered that the maximum operating temperature of some components in the liquid line is 80°C. Therefore, a secondary function of the subcooler was to cool the liquid leaving the condenser to protect the components in the liquid line. The subcooled water inlet temperature was controlled and set according to the subcooler refrigerant outlet temperature. The range of operating conditions are presented in Table 1.

Table 1. List of main components of the HTHP.

Parameters	Setpoint values
Compressor speed	1000, 1230, 1500rpm
Heat source inlet temperature	72, 82, 92, 105°C
Heat sink temperature	133-135°C
Superheating degree setpoint	8-10 K
ΔT Subcooler	50–70 K

4. Experimental setup

The characterization of the HTHP for the Chester project system has been performed in a water-to-water heat pump testing rig in TECNALIA's thermal energy laboratory facilities. This testing rig is used to test heat pump components for high temperature applications (up to 160°C) and heating capacities up to 300kW. The prototype has been manufactured according to safety regulations 2014/68/EU, EN 16084:2011 and EN 378:2016.

The HTHP prototype mainly comprises a compressor, a condenser, a subcooler, an expansion device, and a rack of evaporators. Additional auxiliary components are included in the refrigerant circuit in order to protect the main components and to operate the heat pump safely.

In the suction line, a suction separator is installed to ensure only refrigerant in vapor state is entering the compressor. At the discharge line, a muffler is installed to minimize pressure pulsations. After the condenser a liquid receiver is positioned to accumulate the liquid refrigerant during partial load operation. In the liquid line, a filter/drier is used to protect the expansion device from debris and to maintain the fluid dry. A solenoid valve is mounted to stop liquid migration into the evaporator during off-cycles. Finally, sight glasses are installed in both the suction and liquid lines to control visually the state of the fluid.

The working fluid charged in the circuit is the R-1233zd(E) which is a low GWP fluid and its critical temperature is 165.6°C [9], [10]. A compressor able to operate at very high temperatures has been selected. The compressor is the HBC511 model, manufactured by Viking Heat Engines and can operate at temperatures up to 215°C [11]. There is available study in the literature about the performance of the HBC511 compressor operating with other fluids such as HFO-1336mzz(Z) and R-245fa [12], but none with HCFO-1233zd(E).

Part of the pipelines of the refrigeration cycle and the heat exchangers were kept uninsulated or with removable insulation for visual control, thermography and material monitoring. This causes drop of the global performance of the system, however, the equipment and personnel safety are prioritized.

The list of the main components including the model and manufacturer is presented in Table 2 and the configuration of the proposed HTHP is presented in Fig. 3.

Table 2. List of main components of the HTHP.

Component	Manufacturer	Model
Compressor	Viking Heat Engine	HBC511
Inverter	Siemens	G120
Lubricant	Fuchs	SEZ320
Evaporator #1	SWEP	B80Hx30
Evaporator #2	SWEP	B120Tx30
Condenser	SWEP	B25THx50
Subcooler	SWEP	B86Hx57
Expansion device	Danfoss	ETS12.5
Liquid receiver	Bitzer	FS152
Suction accumulator	Emerson	A17
Discharge muffler	ESK	GDX
Filter/dryer	SANHUA	DTG/L

The secondary fluid circuits consist of four different closed water loops, for the condenser, the subcooler, the evaporators and for the compressor cooling system. The water loop of the condenser is connected to the laboratory cooling system which consists of a buffer tank of 1 m^3 volume, a water cooler, a three-way valve and a water pump driven by an inverter. The subcooler is connected to the medium temperature water loop of the laboratory which is cooled by a geothermal system. The water to the evaporators is heated by a gas boiler and the control is achieved via a secondary loop and a three-way valve. The water loop of the compressor cooling circuit is pumped via a small water pump of 35 W and the water is cooled in a copper pipe coil.

4.1. Monitoring and data logging

Temperature, pressure and flow rates values are measured by sensors in the refrigerant circuit and the four water loops. All data is logged every 1 second by the acquisition system of the laboratory and recorded in a

computer. The datalogging period is considered when the temperature, pressure and flow rate values have been in steady state for a minimum period of time of 10 minutes. The data stored in these periods is averaged and used for the data analysis.

The temperature values in the refrigerant circuit are measured with 4-wire RTD PT100 1/3 DIN sensors custom made by TC-direct. The sensors are positioned in stainless steel thermowells in a counter-current position at the inlet and outlet of each of the main components. Pressure is measured with pressure transducers SPKT*D made by Carel. Two different measure ranges are used depending on the location of measurement whether to be in low- or high-pressure side. Refrigerant mass flow rate is monitored by the Coriolis meter SITRANS FC410 made by SIEMENS.

The temperature in the water loop is measured by six 4-wire PT100 class 1/10 DIN sensors. They are inserted in thermowells at the water inlet and outlet lines of the heat exchangers. Flow rate of the water in the evaporator, condenser and subcooler is measured via three electromagnetic flow meters Sitrans MAG3100 sensors made by SIEMENS. The range of measurements of the sensors and their uncertainties are presented in Table 2.

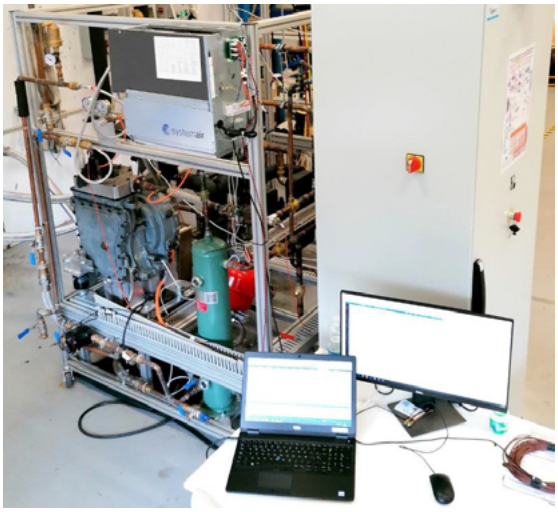

Fig. 2. View of the HTHP testing rig, control panel and datalogging equipment.

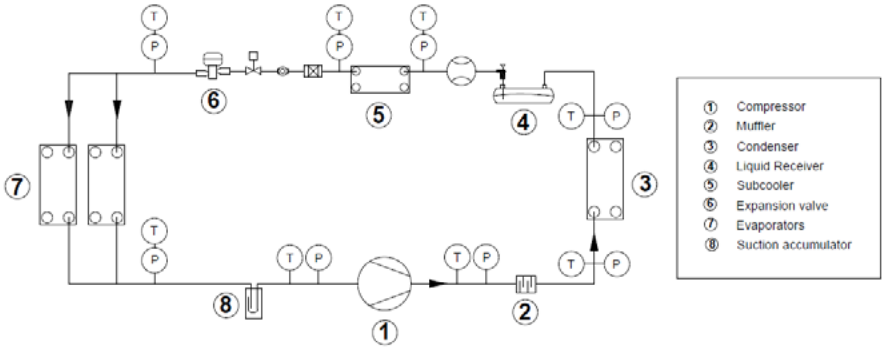

Fig. 3. Schematic diagram of the refrigerant cycle of the HTHP test bench.

Table 2. List of measurement ranges and uncertainties of the monitoring devices.

Measurement	Type	Range	Uncertainty
Temperature - water	PT100, 1/10 DIN	-50 +200°C	±(0.03 °C+0.5%)
Temperature - refrigerant	PT100, Class A	-50 +200°C	±(0.15 °C+0.2%)
Pressure	Transducer	-0.5 to 7 bar / 0 to 30 bar	±0.24% FS
Mass flow – water	Electromagnetic	5-100 l/min	±1.5% FS
Mass flow - refrigerant	Coriolis	20 to 6400 kg/h	0.1% FS
Power	Analyzer	10 to 520 VAC / 40 to 70 Hz	±1% FS

5. Experimental results

The results of the testing campaign are used to study the performance of the HTHP under the Chester system operating conditions and to evaluate the compressor´s performance. The obtained results are considered for the optimization of the HTHP prototype for its integration with the LH-TES and the SH-TES in a CHEST system.

The cooling capacity of the HTHP was calculated for both evaporators considering a single water inlet and outlet. The capacity of both in-parallel connected evaporators ranged from 27.5 to 68.6 kW. The superheating degree was set through the controlled at 8 K and the actual value measured ranged from 7.5 to 8.7 K. Water inlet and outlet temperatures in the evaporator ranged from 72 to 105°C and from 66 to 95°C respectively.

The function of the condenser in the CHEST system will be delivered by the phase change material within the LH-TES. The heating capacities values calculated in this study are used for the sizing of the storage systems. The heating capacity delivered to the condenser´s water loop was calculated between 12.1 kW and 42.3 kW. Water temperatures ranged from 123 to 128°C and 130 to 133.5 °C in the condenser inlet and outlet respectively. The average water temperature difference was approximately 5.5 K. The water pumps used limited the further drop of the temperature difference, therefore they will be substituted for the next testing campaign. In the refrigerant side the condenser inlet and outlet temperatures were measured between 143 to 133 °C and 135 to 132 °C, respectively. The subcooling at the condenser was calculated from 1 to 1.6 K.

The heat transferred to the water in the subcooler ranged from 10.8 to 29.2 kW at water outlet temperatures from 75.8 to 114.6 °C. The subcooling degree measured in the subcooler ranged from 50 to 68 K. The liquid refrigerant leaving the subcooler was maintained below 80 °C due to components' temperature limitations.

Water flow rate and pressure were maintained steady in all loops at 1.32, 0.93, and 0.19 kg/s in the evaporator, condenser and subcooler, respectively. The pressure in the water loops was maintained above 3 bar-g.

The evaporating temperatures and pressures for all tests ranged from 64.1 to 93.6 °C and 4.4 to 9.1 bar-a, respectively. Since the condensing temperature was fixed above 133 °C, the condensing pressure was very stable at approximately 20.4 bar-a.

It should be mentioned that the heat losses in the refrigeration cycle were very high due to poor insulation at the main sections of the piping, specially in the high-pressure side. The existing insulation material in the test bench had to be removed because it presented some irregularities due to high temperature operation such as outgassing and hardening. Furthermore, the vibrations coming from the compressor caused failure in the soldering and some parts of the pipeline were maintained uncovered for material monitoring purposes. This have caused considerable heat losses which are calculated to be between 10 to 26% of the heat produced. The heat transferred to the cooling water of the compressor crankcase is also included in the mentioned percentage and it has to be further evaluated.

In Fig. 4 the COP of the HTHP and power consumption are presented over the temperature lift which is the difference between the condensing and evaporating temperature. As expected, the highest COP value of 7.2 is seen during 1000 rpm speed and at low temperature lift. For 1230 and 1500 rpm the maximum values resulted in 6 and 5.4, respectively, under temperature lifts of approximately 30 K. The lowest COP values for the three compressor speeds were between 3.8 and 4.1 and are observed at temperature lift of 60 K, approximately.

According to the Chester prototype site requirements the compressor must operate consuming below 15 kWe of power (W_{in}). The results presented in Fig. 4 show that the power consumption of the HTHP, which consists of the compressor and inverter consumption, ranged from 5.5 to 13.2 kW. Therefore, the HTHP can run at any speed up to 1500rpm when integrated to the CHEST system.

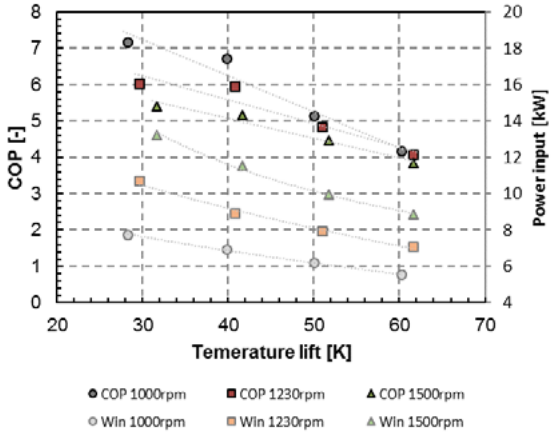

Fig. 4. Performance of the heat pump (COP) and the power consumed (W_{in}) by the compressor and inverter versus the temperature lift.

5.1. Compressor performance

The compressor suction and discharge temperatures ranged from 71.2 to 101.2 °C, and from 136.6 to 149.4 °C, respectively. The suction and discharge pressures ranged from 4.2 to 8.7 bar-a, and 20 to 21.9 bar-a, respectively. Fig. 5 presents the measured mass flow rates for each compressor speed over the evaporating temperature. The lowest mass flow rate was 0.14kg/s, which was measured at compressor speed of 1000 rpm. The mass flow rate increased with the compressor speed to 0.17 and 0.19 kg/s for 1230 and 1500 rpm, respectively. For speed of 1230 rpm the mass flow rate ranged from 0.17 to 0.36 kg/s and for compressor speeds of 1500 rpm the mass flow rate ranged from 0.19 to 0.40 kg/s.

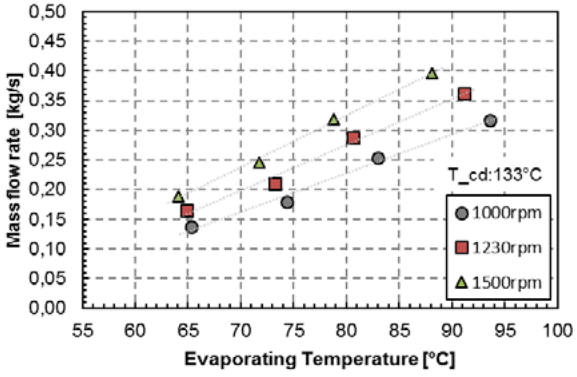

Fig. 5. Refrigerant mass flow rate values at condensing temperature 133°C.

The lowest pressure ratio was calculated at compressor speed of 1000 rpm and heat source of 72 °C. The maximum pressure ratio recorded was 4.9 at 1500 rpm and heat source temperature of 105 °C. The performance of the compressor is further evaluated through the isentropic and volumetric efficiencies. In Fig. 6 both the isentropic and volumetric efficiencies are presented over the pressure ratio. The isentropic efficiency was calculated by Equation 4. The highest value of the isentropic efficiency was 82.4% which corresponds to compressor speed of 1000 rpm and pressure ratio of 4.5. The lowest value is calculated for operation at 1500 rpm speed and pressure ratio of 2.9.

The volumetric efficiency was calculated by Equation 5 and the results ranged from 70.9 to 85.4%. The calculated points show a pattern that splits the values depending on the evaporating temperature and therefore on the mass flow rate.

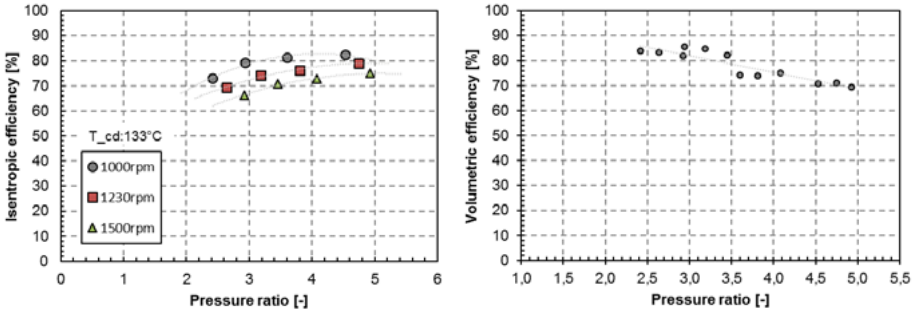

Fig. 6. The isentropic efficiency of the compression phase at different compression speeds (left); and the volumetric efficiency of the compressor (right).

In this study the main objective is to evaluate the performance of the compressor working with R-1233zd(E) to facilitate the selection of the main components of the CHEST system's HTHP. The COP of the HTHP was calculated using Equation 3 but the results are not used for characterization purposes of the testing bench due to the low quality of insulation used. Moreover, the evaporators have not been sized for this specific compressor, therefore, are not optimum for this configuration. However, the results of performance are promising, and they can be used for comparison purposes with future tests.

6. Data reduction and simulations

The presented results have been calculated using equations and calculation software packages such as Microsoft Excel and REFPROP [13]. Both the cooling and heating capacities of the HTHP were calculated using the Equations 1 and 2 described below.

$$Q_w = m_w \cdot c_{p,w} \cdot \Delta T_w \quad (1)$$

$$Q_r = m_r \cdot \Delta h_r \quad (2)$$

Where the heating/cooling capacity of the heat pump (Q_w) is the result of the water mass flow rate (m_w) by the specific heat capacity ($c_{p,w}$) by the temperature difference between the water inlet and outlet of the heat exchanger (ΔT_w). The heating/cooling capacity in the refrigerant side (Q_r) is the refrigerant mass flow rate (m_r) by the enthalpic difference (Δh_r) of the fluid between the inlet and outlet of the refrigerant in the heat exchangers.

The COP is calculated from the ratio of the sum of heating capacities in the condenser and subcooler (Q_{out}) over the power consumed (W_{in}). by both the compressor and the inverter (Equation 3)

$$COP = \frac{Q_{out}}{W_{in}} \quad (3)$$

The isentropic efficiency is calculated from the ratio of the enthalpy difference in the compression process assuming an isentropic compression to the experimental enthalpy difference of the compression stage as presented in Equation 4. The isentropic compression enthalpy is calculated from the difference between the isentropic enthalpy at the discharge ($h_{dis,is}$) and the enthalpy at the suction (h_{su}). The actual compression enthalpy is calculated by the difference between the actual enthalpy at the discharge (h_{dis}) and the enthalpy at the suction of the compressor.

$$\eta_{is} = \frac{h_{dis,is} - h_{su}}{h_{dis} - h_{su}} \quad (4)$$

The volumetric efficiency is calculated by Equation 5, and is the ratio of the refrigerant mass flow rate (m_r) by the specific volume at the suction (V_{su}), over the theoretical volume of gas displaced by the piston (V_{displ}) multiplied by the frequency per second and by the number of pistons (n). The volumetric displacement of the single piston compressor considered for this study is 511cm^3. The specific volume of the gas at the suction line is calculated using REFPROP [13].

$$\eta_{vol} = \frac{m_r . V_{su}}{V_{displ} \cdot (f/60) \cdot n} \quad (5)$$

7. Conclusions

The performance of a HTHP working with a low-GWP working fluid has been investigated. The HTHP is designed to be part of a CHEST system where its function is to charge a LH-TES at temperatures above 133°C. Additional sensible heat from the subcooler charges a SH-TES system resulting in a subcooling degree between 50-68 K.

Water was used as secondary fluid and the mass flow rates were maintained steady during the testing campaign. The water inlet temperatures set for the testing campaign ranged from 72°C to 105°C, and the condenser water outlet temperature ranged from 133 to 135°C. For each testing condition three compressor speeds were tested, 1000, 1230, and 1500rpm.

The capacity of both evaporators in parallel configuration was measured as a sum and ranged from 27.5 to 68.6 kW. The heating capacity delivered to the water in the condenser was estimated from 12.1 to 42.3 kW. The subcooler's heating capacity was calculated from 10.8 to 29.2 kW with a temperature difference in the water-side from 13 to 35 K.

Evaporating and condensing temperatures ranged from 64 to 94°C and 133 to 125.8 °C, respectively. The compressor suction temperatures ranged from 71.2 to 101.2 °C, and the discharge temperatures from 136.6 to 149.4 °C, respectively. The suction pressures ranged from 4.2 to 8.7 bar-a and the discharge pressures remained stable as expected between 20 to 21.9 bar-a. The superheating degree value resulted from 7.5 to 8.7 K and the total subcooling degree achieved in both the condenser and subcooler resulted from 50.7 to 69.4 K. Using the subcooler was crucial to protect the components in the liquid line and maintain them below their maximum operating temperatures (80°C).

The operating pressure ratios of the compressor were calculated from 2.4 to 4.9. The lowest compressor speed presented higher isentropic efficiency ranging from 73 to 82%. While for 1500 rpm, the isentropic efficiency ranged from 66 to 75%. The highest volumetric efficiency was 85% and was recorded under the 1000 rpm compressor speed at high pressure ratio conditions. However, the volumetric efficiency was weakly influenced by the compressor speed since the difference between the volumetric efficiency values resulted from 0.5-1.4% at each operating condition.

The COP of the HTHP tested resulted in values from 3.8 to 7.2. The maximum values were recorded as expected at the lower compressor speeds, 1000 rpm and 105 °C heat source temperature. The lowest performance values resulted under heat source temperature of 72 °C and temperature lift of 60 K.

Power consumption of the HTHP that consisted of the consumption of the compressor and the inverter was measured in the range of 5.5 to 13.2 kW. Since the power supply in the Chester prototype site is limited to 15kWe the results show that there is no limitation for any of the compressor speeds tested.

Finally, actualization of the control algorithm is necessary to control the operation range of the HTHP coupled to the CHEST system. Different operating modes will be implemented into the control and will be tested individually. In addition, further optimization of the thermal insulation of the refrigerant pipeline must be conducted to increase the efficiency of the cycle.

Acknowledgements

The authors would like to express their gratitude to Viking Heat Engines for their technical support and to Fuchs Petrolub SE for the lubricant supplied for this specific application. This work is part of the European Union's Horizon 2020 research and innovation program CHESTER (Grant agreement No. 764042).

References

[1] Eurostat. (2016). Eurostat. Retrieved October 10, 2019, from https://ec.europa.eu/eurostat/web/products-eurostat-news/-/DDN-20180921-1

[2] Zhang, C., Wei, Y. L., Cao, P. F., & Lin, M. C. (2018). Energy storage system: Current studies on batteries and power condition system. Renewable and Sustainable Energy Reviews, 82(July 2017), 3091–3106.

[3] Irena, International Renewable Energy Agency. (2012). IRENA-IEA-ETSAP Technology Brief 5: Electricity Storage, (April).

[4] Irena, International Renewable Energy Agency. (2017). Electricity storage and renewables: Costs and markets to 2030.

[5] Steinmann, W. D. (2014). The CHEST (Compressed Heat Energy STorage) concept for facility scale thermo mechanical energy storage. Energy, 69, 543–552.

[6] Frate, G. F., Antonelli, M., & Desideri, U. (2017). A novel Pumped Thermal Electricity Storage (PTES) system with thermal integration. Applied Thermal Engineering, 121, 1051–1058.

[7] Jockenhöfer, H., Steinmann, W. D., & Bauer, D. (2018). Detailed numerical investigation of a pumped thermal energy storage with low temperature heat integration. Energy, 145, 665–676.

[8] Weller T., Jockenhöfer H., Fiss M., B. D. (2019). Detailed design of the high temperature TES laboratory prototype. Retrieved from https://www.chester-project.eu/public-documents/

[9] Honeywell Brochure. (2013). Honeywell Refrigerants Improving the Uptake of Heat Recovery Technologies. Honeywell Brochure, 53(9), 1689–1699.

[10] Gil, B., & Kasperski, J. (2018). Efficiency evaluation of the ejector cooling cycle using a new generation of HFO/HCFO refrigerant as a R134a replacement. Energies, 11(8), 1–18.

[11] Viking Heat Engines. (2018). HBC 511 - Data Sheet 1.1. Retrieved May 10, 2018, from www.vikingheatengines.com/upl/files/144869

[12] Nilsson, M., Nes, H., & Kontomaris, K. (2017). Measured performance of a novel high temperature heat pump with HFO-1336mzz(Z) as the working fluid. In 12th Heat Pump Conference. Rotterdam: IEA Heat Pump Conference.

[13] Lemmon, E. W., Bell, I. H., Huber, M. L., & McLinden, M. O. (2018). NIST Standard Reference Database 23: Reference Fluid Thermodynamic and Transport Properties-REFPROP. Gaithersburg: National Institute of Standards and Technology.